Spectroscopic Measurements of Argon Plasma Formation by a High-Intensity Lithium Ion Beam

J. E. Bailey,[1] H. K. Chung,[2] A. L. Carlson,[1] D. Cohen,[2] D. J. Johnson,[1] P. Lake,[4] J. J. MacFarlane,[2] P. Wang,[2] and D. R. Welch[3]

[1]*Sandia National Laboratories, Albuquerque, New Mexico 87185*
[2]*Fusion Technology Institute, University of Wisconsin, Madison, Wisconsin 53706*
[3]*Mission Research Corporation, Albuquerque, New Mexico 87106*
[4]*K-Tech Corporation, Albuquerque, New Mexico 87110*

(Received 3 August 1998)

We describe the first measurements of plasma formation by a 20 nsec, 9 MeV, 20 kA/cm^2 Li^{+3} ion beam injected into 2-Torr argon, conditions similar to inertial-fusion ion-beam transport requirements. A new visible-spectroscopy diagnostic exploits ion-beam-excited Ar II transitions to measure the time-resolved plasma electron density (10^{15} cm^{-3}–10^{16} cm^{-3}) and temperature (1–2 eV) during the initial breakdown phase. Stark broadening and line intensity ratios are used as diagnostics after the plasma forms. Comparisons with computer simulations examine intense-beam effects important for the transport of light- and heavy-ion beams. [S0031-9007(98)08301-X]

PACS numbers: 52.40.Mj, 52.58.Ei, 52.58.Hm, 52.70.Kz

Light- and heavy-ion beams share promise as drivers for inertial fusion energy (IFE) [1]. Ion-driven IFE employs a several-meter standoff of the final focusing apparatus from the fusion capsule. This mitigates damage, enables beam bunching, and is essential for repetitive operation. One of the most desirable ways of transporting the beam to the target is injection into gas [2]. The beam ionizes the gas, forming a plasma that provides charge and controllable current neutralization. This method requires an understanding of plasma production by high-intensity nonprotonic ion beams.

This Letter describes the first measurements of plasma production by an ion beam approaching the parameters (35 MeV, 12 kA/cm^2, Li^{+3}) expected [2] in the transport region of an IFE facility. In our experiments a 9 MeV, 20 kA/cm^2 Li^{+3} beam deposits 8 TW/g in 2-Torr Ar, about a 40 times higher specific deposition than in previous beam transport experiments [3]. The high intensity enables the first studies of beam transport in a plasma that becomes fully ionized, in contrast to the typically 1% ionization fractions previously obtained. A variety of visible-spectroscopy techniques, including a new method developed here, were used to measure the electron density (n_e) and temperature (T_e). Comparisons of the data with $2\frac{1}{2}$-dimensional hybrid particle-in-cell (PIC)/fluid electromagnetic computer simulations show that stepwise ionization, from the Ar I ground state to the Ar I excited states and then to Ar II, must be accounted for to achieve accurate predictions of the argon ionization kinetics.

Light-ion fusion requires charge and current neutralization because otherwise the approximately 1 MA beam currents and 10^{13} cm^{-3} beam densities produce self-fields that disrupt the beam [4]. Thus, understanding of and control over the ionization processes which determine the transport plasma conductivity are necessary. Self-pinched transport [5], the most promising scenario presently considered, requires a finite net current to contain the beam. Detailed knowledge of the gas breakdown is needed to determine the net current.

Heavy-ion fusion may use ballistic final transport in 10^{-3}–10^{-2} Torr background gas, but this still requires consideration of gas ionization since partial beam neutralization and beam stripping can occur [6]. Self-pinched transport is more desirable, if the complex issues of multiple charge state beams and plasma formation can be addressed. The present Li^{+3} measurements assist heavy-ion research by benchmarking simulations of the plasma formation and developing diagnostic methods which may be used in higher-intensity heavy-ion experiments.

Previous investigations of gas breakdown by ion beams were limited by relatively low beam intensities. Xenon ionization by a 3.8 MeV Kr^{+1} beam depositing 0.0015 TW/g was measured spectroscopically [7]. An initial feasibility study using spectroscopic measurements of 1–3 TW/g proton beam transport in Ar was reported [8], but the full exploitation of such measurements was not realized. In later proton beam experiments [3] at 0.2 TW/g, measurements of net current were successfully compared with computer simulations. However, in Ref. [3] the ~25 nsec time resolution prevented analysis of the initial breakdown.

Injection of a high-intensity ion beam into gas creates an initially non-Maxwellian electron distribution determined by the ion impact secondary electron distribution [9], knock-on collisions, and the large electric and magnetic fields associated with the beam. As the gas breakdown proceeds, the electrons approach an approximately Maxwellian distribution, although a small fraction are expected to remain in a high-energy tail. Models [10] and simulations [11] predict an initially high *thermal* electron temperature T_e that eventually relaxes to a value that is a fraction of the target atom ionization potential. A goal for

the present work is to begin the experimental evaluation of these processes in the high-intensity regime.

These experiments were conducted using a cylindrically symmetric applied-magnetic-field ion diode [12] powered by the Particle Beam Fusion Accelerator II to accelerate a radially inward-directed singly ionized lithium beam (Fig. 1). The beam enters the 2-Torr-argon gas cell, strips into the Li^{+3} charge state, and is transported ~13 cm to the target located on the cylinder axis. The beam current density and kinetic energy (Fig. 1) were measured using a suite of diagnostics located at the gas cell boundary and at the diode axis [12]. The properties of the gas cell plasma are determined using time-resolved visible spectroscopy [13]. The 4-mm-diam line of sight (LOS) is aligned parallel to the cylindrical axis at a radius of 4 cm (Fig. 1). The spectra were recorded with 1.6 Å spectral resolution over the 4300–4700 Å range and a time resolution of approximately 1 nsec, although in the present analysis 3 nsec lineouts are used to improve the signal quality. The timing precision is ±2 nsec with respect to the beam measurements. The line properties were measured by fitting Voigt profiles to each line using the ROBFIT [14] code. The data below account for the measured instrument sensitivity. Polarization effects are expected to be small [15] and were not included.

The spectral intensities are interpreted with a time-dependent collisional radiative (CR) model that treats 627 Ar I-VII atomic levels self-consistently with radiation transport [16]. Collisional processes involving assumed-Maxwellian thermal electrons, the ion beam, and nonthermal electrons are included. We assume that the plasma ion and thermal electron temperatures are the same and that the nonthermal electron energy distribution (E_{nt}) scales as $1/E_{nt}^2$, as suggested by the computer simulations described below. We truncate the nonthermal distribution at an end point energy of 2 keV, since few electrons appear at higher energies in the simulations.

We observe Ar II emission (Fig. 2) from the $4p\,^2P$, $4p'\,^2F$, and $4p\,^4D$ levels simultaneously with the arrival of the beam front at the LOS location ($t = 0$ is defined to be when the current density reaches 1% of its peak). Later, emission is also observed from the Ar II $4p\,^2S$, $4p\,^4P$, $4f$, $5s$, and $5s'$ states. Note that the levels share the $1s^2 2s^2 2p^6 3s^2 3p^4$ core, but the ^1D core term is designated with a "prime" and the ^3P core term is unprimed. No Ar I emission was observed, due to the relatively low Ar I transition probabilities. Innershell Ar II emission was also not observed, since these transitions are at wavelengths below 1000 Å. Several as yet unidentified spectral lines which appear at about $t = 15$ nsec have been tentatively associated with Ar III transitions.

We have developed a new plasma diagnostic for the $n_e \sim 10^{15}$ cm^{-3} regime that is characteristic of the first few nsec of the breakdown. During this phase, the ionization fraction is low and the plasma predominantly consists of ground state Ar I atoms. Comparisons of measured cross sections [15,17,18] show that, in this case, the dominant mechanism populating the Ar II excited states is simultaneous beam ion impact ionization/excitation from the Ar I ground state, rather than a two step process in which an Ar I atom is first ionized into the Ar II ground state and subsequently excited. The importance of this mechanism was previously recognized [19] in analysis of electron beam excited spectra [20], although, to our knowledge, plasma diagnostics using this process have not been mentioned before. During this phase, n_e is so low that very little population redistribution occurs before the levels spontaneously decay. As n_e rises, collisional redistribution among the Ar II excited states increases and they approach local thermodynamic equilibrium (LTE) with each other. In this partial LTE condition (PLTE) [21] the relative excited state populations are determined by the level energy, T_e, and the statistical weight, although the excited states are still substantially enhanced over LTE with respect to the Ar II ground state. The basis of the diagnostic developed here

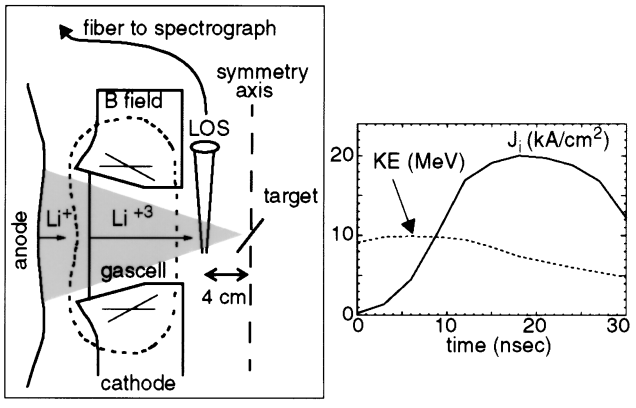

FIG. 1. Schematic diagram of the experiment. The measured ion current density (J_i) and kinetic energy (KE) are shifted to the location of the spectroscopy line of sight, accounting for the time of flight and the beam ion trajectories.

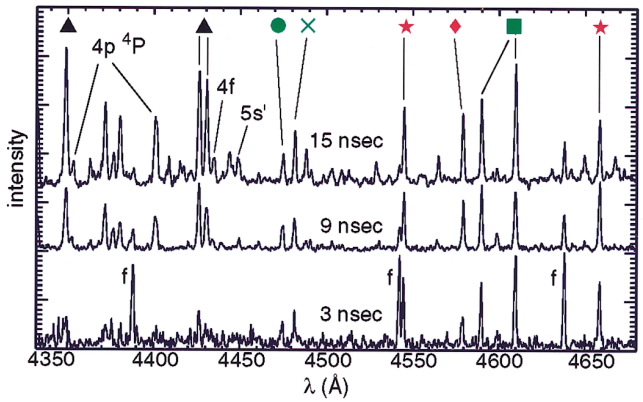

FIG. 2(color). Sequence of measured spectral lineouts, each averaging over 3 nsec. The intensities are normalized so that the intensity of the 4658 Å line is constant. The lines labeled f are wavelength fiducials. The red symbols indicate Ar II $4p$ doublets (star: ^2P; diamond: ^2S), the green symbols indicate Ar II $4p'$ doublets (square: ^2F; cross: ^2D; circle: ^2P) and the black symbols indicate Ar II $4p$ quartets (triangle: ^4D).

is that the simultaneous ionization/excitation process favors population of $4p$ and $4p'$ doublet levels over the $4p$ quartets. Thus, transitions from doublet levels are initially bright compared to quartet levels. The quartet/doublet intensity ratios change as the level populations approach PLTE. The time history of the quartet/doublet line ratios therefore reflects n_e and T_e, since they control how fast collisional equilibration among the excited states occurs. The variation in the quartet/doublet ratios with time is evident in Fig. 2.

The transition from domination by simultaneous ion impact ionization/excitation of the Ar II excited states to PLTE is illustrated by Boltzmann plots [21], using the fact that, if PLTE exists, a plot of $\ln[P_{21}I_{21}\lambda_{21}/g_2A_{21}]$ versus E_2 should give a straight line of slope $-1/T_e$, where g_2 is the statistical weight of the upper level, A_{21} is the transition probability from level 2 to level 1, λ_{21} is the wavelength, I_{21} is the intensity, and E_2 is the energy of the upper level. P_{21} is an opacity correction based on a probability of escape approximation [22] and assuming LTE holds among the lower levels. A Boltzmann plot using Ar II line intensities measured at $t = 3$ nsec is shown in Fig. 3(a). The scatter of the points clearly indicates that PLTE does not hold at this time. Comparison of the symbols representing transitions from different terms with a CR model calculation [Fig. 3(b)] shows that the calculation reproduces the *exact way* that the data deviates from PLTE. This is achieved only when the simultaneous ionization/excitation process is included in the model, providing strong evidence that this mechanism is in fact responsible for the early phase relative line intensities.

The possibility of PLTE among the excited states led Jayakumar and Fleischmann [23] to suggest that LTE-based diagnostics, such as the Boltzmann plot method for

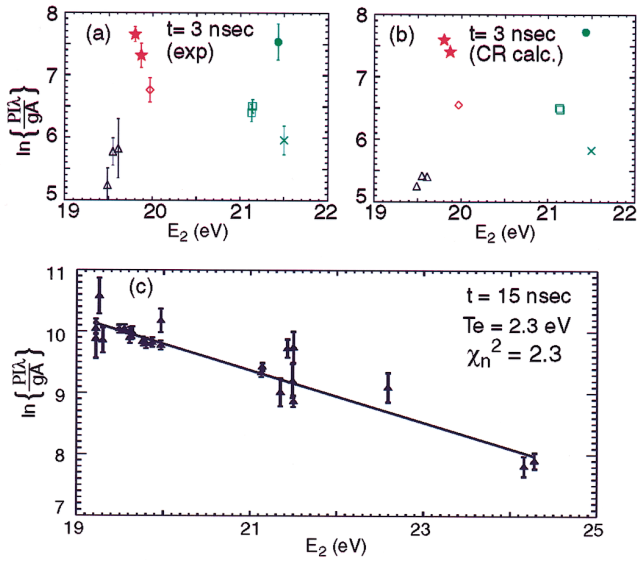

FIG. 3(color). Boltzmann plots from the initial nonthermal phase of the experiment (a) compared to a CR calculation (b). The line symbol notation is the same as in Fig. 2. An experimental plot from the later (partial LTE) phase is shown in (c).

temperature [21], could be applicable even in the presence of fast particles. This idea was successfully used for spectroscopy of an electron beam generated plasma [20]. Collisional radiative calculations for the n_e and T_e range in our experiment confirm that PLTE among all of the Ar II excited states is a good approximation after about 15 nsec. A Boltzmann plot using data from $t = 15$ nsec [Fig. 3(c)] exhibits a straight-line fit that is consistent with PLTE. Collisional radiative calculations also show that the doublet levels equilibrate among themselves prior to reaching equilibrium with the quartet levels. The temperatures from 9-12 nsec are derived using the doublet levels only, and the temperatures from 15–30 nsec are derived from all of the lines (Fig. 4). These results are discussed below.

The plasma conditions during the initial breakdown are determined by comparing measured quartet/doublet line intensity ratios with CR calculations. An iterative procedure is required because the plasma parameters change on a time scale comparable to the atomic processes. The time-dependent ion beam current density and kinetic energy are input using the measured values. The nonthermal electron fraction was assumed to be 1% initially, consistent with the simulations described below. The impact of other assumptions for the nonthermal electron fraction will be discussed elsewhere. Given these inputs and some hypothesis for the thermal electron temperature T_e, we then calculate the thermal electron density n_e, the level populations, and the line intensity ratios. By comparing to the measure quartet/doublet line ratios and iterating, we determine a family of n_e and T_e time histories that are consistent with the data. Thus, we set bounds on n_e and T_e. Out of this family the best fit to the data was obtained using the histories shown as solid lines in Fig. 4. A comparison of measurements and the "best fit" CR calculation for two representative quartet/doublet line ratios are shown in Fig. 5. Good agreement was obtained for *all* of the measured quartet/doublet line ratios, while maintaining consistency between the CR T_e hypothesis and the Boltzmann plot T_e measurements, implying that the best fit line ratio measurements

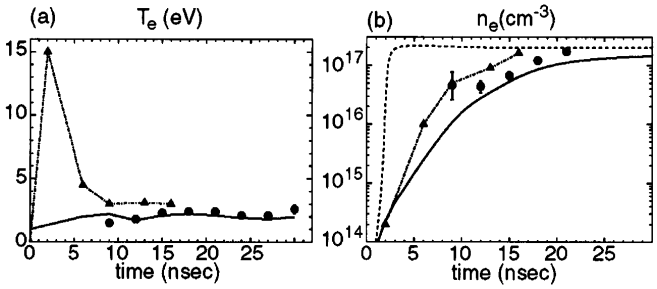

FIG. 4. Plasma electron temperature (a) and density (b) as a function of time. The T_e and n_e values determined with the Boltzmann plot and line profile analysis, respectively, are shown with circles. The experiment values measured using the quartet/doublet line ratios are shown with solid lines. The dot-dashed lines with triangles represent IPROP simulation results. The dashed n_e curve is the result calculated with the CR code using the IPROP T_e.

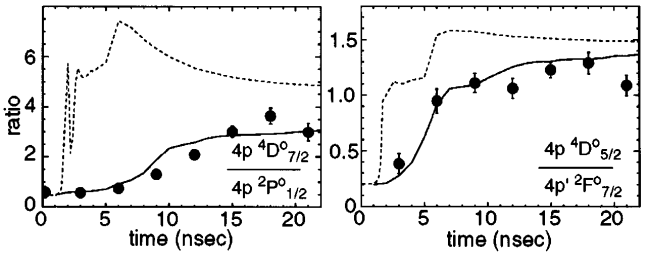

FIG. 5. Plasma diagnostic line ratios from the experiment (circles), the best fit CR calculation (solid line), and a CR calculation using the IPROP simulation T_e (dashed line).

(solid curves in Fig. 4) are a good representation of the experiment.

A further cross-check on these results was obtained by using detailed fits of spectral profiles to self-consistently determine n_e from Stark broadening [24] and the absolute line opacities from the relative linewidths and intensities. This required higher spectral resolution, reducing the sensitivity and limiting observations to the 9–21 nsec time period. The values of n_e obtained from the profile analysis (Fig. 4) agree reasonably well with the line ratio measurements, especially considering that the high resolution spectrum was recorded in a different accelerator discharge. Details of these results will be presented elsewhere.

The measurements enable comparisons with $2\frac{1}{2}$-dimensional hybrid PIC/fluid computer simulations performed with the IPROP code [11]. IPROP uses a PIC treatment for the beam ions and the nonthermal plasma electrons and a fluid treatment for the thermal plasma. The energy deposition, fields, and plasma conditions are calculated self-consistently, but the present atomic model includes only the Ar I and Ar II ground states. The thermal electron density predicted by the simulations agrees to within a factor of 2–4 with the experimental results (Fig. 4). The thermal electron temperature for $t > 9$ nsec also agrees within a factor of 2. However, the duration ($\sim$4 nsec) of the initial spike in T_e is inconsistent with the data. The CR calculations using the simulation T_e history result in rapid electron density growth [Fig. 4(b)] and time histories of the quartet/doublet line ratios (Fig. 5) which are clearly inconsistent with the measurements. Further comparison of CR calculations with the measured quartet/doublet ratios show that, if such an initial T_e spike exists, its duration must be less than about 1 nsec. The duration of this initially high thermal T_e spike depends on the initial non-Maxwellian energy distribution, the persistence of high-intensity beam processes that continue to produce non-Maxwellian electrons, and the thermal electron density (n_e) growth rate. Differences between the idealized simulation beam and the actual beam, such as a possible beam foot that could cause preionization, contribute to the initial T_e discrepancy. However, it is likely that this discrepancy is at least partially due to the simplified atomic model in the simulations. At present, IPROP does not include stepwise ionization from the Ar I ground state to the Ar I excited states and then to Ar II. This unphysically slows the growth of n_e and allows T_e to remain high longer, since the energy deposited by the beam is distributed over fewer particles. Work is in progress to embed a CR code within IPROP in order to improve the accuracy of both the ionization kinetics and the resulting plasma conductivity. The experimental methods developed here and these improved simulations can then be considered for future studies at the lower gas pressures needed for self-pinched transport.

We thank the PBFA II operations crew and D. F. Wenger for technical assistance. We are also grateful to Y. Maron, E. J. McGuire, T. A. Mehlhorn, B. Oliver, and C. Olson for many useful discussions, and to D. L. Cook, R. J. Leeper, and J. P. Quintenz for support and encouragement. Sandia is a multiprogram laboratory operated by Sandia Corporation, a Lockheed Martin Company, for the U.S. Dept. of Energy under Contract No. DE-AC04-94AL85000.

[1] *Nuclear Fusion by Inertial Confinement,* edited by G. Vellarde, Y. Ronen, and J. M. Martinez-Val (CRC Press, Ann Arbor, 1993).
[2] C. Olson et al., *Proceedings of the 16th IAEA Fusion Energy Conference, Montreal, 1996* (IAEA Press, Vienna, 1997), p. 195.
[3] F. C. Young *et al.,* Phys. Rev. Lett. **70**, 2573 (1993).
[4] C. Olson, J. Fusion Energy **1**, 309 (1982).
[5] D. R. Welch and C. L. Olson, Fusion Eng. Des. **32–33**, 477 (1996).
[6] D. A. Callahan, Fusion Eng. Des. **32–33**, 441 (1996).
[7] J. Jacoby *et al.,* Phys. Rev. Lett. **65**, 2007 (1990).
[8] J. E. Bailey *et al., Proceedings of the 9th International Conference on High Power Particle Beams,* edited by D. Mosher and G. Cooperstein (NTIS, Springfield, VA, 1992), p. 903.
[9] M. E. Rudd *et al.,* Rev. Mod. Phys. **64**, 441 (1992).
[10] B. V. Oliver, P. F. Ottinger, and D. V. Rose, Phys. Plasmas **3**, 3267 (1996).
[11] D. R. Welch *et al.,* Phys. Plasmas **3**, 2113 (1996).
[12] D. J. Johnson *et al.,* Laser Part. Beams **16**, 185 (1998).
[13] J. E. Bailey *et al.,* Rev. Sci. Instrum. **68**, 1009 (1997).
[14] R. L. Coldwell and G. J. Bamford, *The Theory and Operation of Spectral Analysis Using* ROBFIT (AIP, New York, 1991).
[15] P. N. Clout and D. W. O. Heddle, J. Phys. B **4**, 483 (1971).
[16] H. K. Chung *et al.,* Rev. Sci. Instrum. **68**, 350 (1997).
[17] D. W. O. Heddle and J. W. Gallagher, Rev. Mod. Phys. **61**, 221 (1989).
[18] J. A. Sanchez *et al.,* Phys. Rev. A **41**, 1392 (1990).
[19] D. B. McGarrah and M. L. Brake, Laser Part. Beams **8**, 507 (1990).
[20] M. Brake *et al.,* J. Appl. Phys. **60**, 99 (1986).
[21] W. L. Wiese, Spectrochim. Acta B, At. Spectrosc. **46**, 831 (1991).
[22] J. P. Apruzese, J. Quant. Spectrosc. Radiat. Transf. **34**, 447 (1985).
[23] R. Jayakumar and H. H. Fleischmann, J. Quant. Spectrosc. Radiat. Transf. **33**, 177 (1985).
[24] S. Pellerin *et al.,* J. Quant. Spectrosc. Radiat. Transf. **57**, 349 (1997).